Electronic Supplementary Information

A Conformational Tweak for Enhanced Cellular Internalization, Photobleaching Resistance and Prolonged Imaging Efficacy

Niranjan Meher,[a] Anil Parsram Bidkar,[b] Debasish Barman,[a] Siddhartha Sankar Ghosh,[b,c]* and Parameswar Krishnan Iyer[a,c]*

[a]Department of Chemistry, [b]Department of Biosciences and Bioengineering, [c]Center for Nanotechnology, Indian Institute of Technology Guwahati, Guwahati-781039, Assam, India

*AUTHOR INFORMATION

Prof. Parameswar Krishnan Iyer
E-mail: pki@iitg.ac.in;
Fax: +91 361 258 2349

Experimental Methods

Materials and Instrumentations: All starting materials and reagents (viz: 1,8-naphthalic anhydride, n-hexylamine, 8-hydroxyquonoline and 6-hydroxyquonoline) were purchased from Sigma Aldrich (INDIA) and were of reagent grade. HPLC grade solvents used in this study were purchased from Fisher Scientific Ltd. and RANKEM. NMR (^{1}H, ^{13}C) spectra were recorded with a Bruker Avance 600 MHz spectrometer. All solutions for ^{1}H and ^{13}C spectra were obtained taking residual solvent signal as the internal reference. Electrospray ionization mass spectrometry (ESI-MS) was recorded on a Waters (Micro mass MS-Technologies) Q-Tof MS Analyzer spectrometer. Microbalance (± 0.1mg) and volumetric glassware were used for the preparation of solutions. UV/vis and PL spectra were recorded on a Perkin-Elmer Model Lambda-750 spectrophotometer and a Horiba Fluoromax-4 spectrofluorometer respectively using 4 mm quartz cuvettes at 298 K. Field emission scanning electron microscopy (FESEM) images were obtained on Sigma Carl ZEISS field emission scanning electron microscope. TEM images were obtained from a JEOL 2100 UHR-TEM instrument, operating at 200 KV. X-ray diffraction (XRD) measurements were performed using Bruker D2 PHASER X-ray diffractometer (10 mA, 30 kV) equipped with Ni-filtered Cu Kα radiation, at a wavelength of 0.154 nm. The samples were scanned in the 2θ range of 5–50^{o} at a scan rate of 1.2^{o} min^{-1}. Single crystal data were obtained with a Bruker SMART APEX diffractometer equipped with a CCD area detector.

Preparation of the Fluorescent Self-Assembly for photophysical studies: Stock solutions of probes (10 mM) were prepared in DMF. The respective fluorescent supramolecular assemblies were prepared by dispersing a certain fraction of the DMF solution of probes (**6HNQ** and **8HNQ**) quickly into milli-Q water. For all the photophysical studies, 20 μM of the dispersed probe solution in 99.8% water has been taken. The resulting dispersed solution was shaken well at room temperature before measurements.

Preparation of FESEM: The morphological analysis of the spontaneously formed supramolecular self-assembly was carried out by FE-SEM analysis. The simple drop-casting technique was performed to prepare the samples. The dilute dispersed solution of the naphthalimide skeletal isomers in 99.8%water-0.2%DMF were drop casted on aluminum foil and were dried in room temperature overnight before analysis.

Theoretical Studies: The electronic properties of both the naphthalimide congeners (**6HNQ** and **8HNQ**) were calculated using density functional theory (DFT). The ground state optimized geometries along with HOMO/LUMO electron density and energy were calculated using B3LYP hybrid functional incorporated in the Gaussian 09 package.[1,2] The 6-31G basis set for all the atoms has been used in all calculations, which offers high-quality outcomes at a reasonable time. The molecules were optimized in both gaseous phase and with solvation (DMSO and water) using CPCM solvation model.

Cell culture: All the cells used in this project were procured from the repository of the National Centre for Cell Science (NCCS) Pune, India. The cells were proliferated to confluence in Dulbecco's modified Eagle's medium (DMEM, Sigma) supplemented with 100 U/mL penicillin, 100 μg/mL streptomycin (GIBCO) and heat-inactivated fetal bovine serum (FBS, GIBCO), and maintained at 37^{o}C in a humidified atmosphere of 5% CO_2 for further cell experiments.

MTT Assay: For assessment of the cytotoxic effect of **6HNQ-MF** and **8HNQ-NR** via MTT [3-(4,5-Dimethyl-2-thiazolyl)-2,5-diphenyl-2H-tetrazolium bromide] assay, various type of mammalian cells like HEK293 (human embryonic kidney), HeLa (cervical cancer), MCF7 (breast cancer) and HepG2 (liver cancer) cells were seeded in 96-well plates at a density of 5×10^3 cells/well. The medium was then replaced by DMEM containing predetermined concentrations of **6HNQ-MF** or **8HNQ-NR**, and then incubated for 24 h. After completion of the treatment for 24 h, the growth medium was aspirated and MTT solution (0.3μg/mL) was added in each well and again incubated for 2h. Cell viabilities were determined by reading the absorbance of the plates at 570 nm with a microplate reader. The cells incubated with DMEM were used as the control. As the DMF stock solution was used for the preparation of fluorescent self-assembly of the probes, the cytotoxicity of various DMF volume fraction used for the preparation of the dispersed nanoaggregate solution was also determined.

Cell Viability Assay: Growth inhibitory properties of the **6HNQ-MF** and **8HNQ-NR** were tested on mammalian cells by MTT assay. Viability assays confirmed the dose-dependent reduction in live cell population. To gain the further insights into the potency of the compounds, IC_{50} concentrations were calculated and are presented in Table S1. From the initial observations it was concluded that, **8HNQ-NR** was more potent as compared to the **6HNQ-MF**. Cell death inducing property of the **6HNQ-MF** and **8HNQ-NR** was further confirmed with propidium

iodide (PI) based flow cytometric assay on IC_{50} concentration treated HeLa cells. Histograms shown in Figure S4e-h showed that the **6HNQ-MF** and **8HNQ-NR** were able to kill the 41.9% and 47.4% cells, respectively.

Table S1. IC_{50} values of **NSIs** for different cells.

Cells	**6HNQ-MF** (μM)	**8HNQ-NR** (μM)
HeLa	45.95 ± 2.10	25.16 ± 1.42
HEK293	82.70 ± 3.45	32.70 ± 1.20
HepG2	26.96 ± 1.35	23.49 ± 0.82
MCF-7	48.07 ± 2.41	22.55 ± 1.54

Cellular uptake: To study the cellular uptake of **6HNQ-MF** and **8HNQ-NR**, HeLa cells were grown on coverslip kept in 6-well plate at a density of 2×10^5 cells/well and incubated in DMEM. Following the attachment, the cells were treated with preformed **6HNQ-MF** or **8HNQ-NR** at 10 μM concentrations and incubated for different time (0-6 h) at 37°C, and further washed using PBS. After incubating the cells for different time, the cells were fixed with 4% of paraformaldehyde solution for 10 min. After that, propidium iodide (PI) was added for another 5 min incubation to locate the nucleus. Later, the cells were washed with PBS and observed using confocal microscopy (CMSM, ZEISS LSM-880).

Mechanism of the Uptake: To study the mechanism of the internalization of the 6HNQ-MF and 8HNQ-NR, HeLa cells were seeded in 96 well plate at 5 x 10^3 cells/well. To confirm the uptake at 4 °C, cells were incubated at 4 °C for 1 h, and then cells were treated with 6HNQ-MF and 8HNQ-NR for 6 hr. For inhibition of the active or energy mediated internalization pathway, Sodium azide treatment was given for 2 h, followed by the 6HNQ-MF and 8HNQ-NR treatment for 6 h. After completion of the treatment, the cells were washed with PBS to remove the free molecules if any. The fluorescence intensities of the 6HNQ-MF and 8HNQ-NR were measured in TECAN multiplate reader.

Uptake Mechanism Briefing: The mechanism of the internalization (passive or active) also plays an important role during the entry of the molecules inside the cells. Almost all the endocytosis pathways are active, or energy dependent processes, and these processes can be blocked by keeping the cells at 4 ˚C, including sodium azide (ATPase inhibitor), which blocks the energy dependent processes. Thus, the uptake mechanism was confirmed by studying the uptake of 6HNQ-MF and 8HNQ-NR in presence of the sodium azide or at 4 ˚C. The uptake

study (Figure S15) shows that the internalization of the 6HNQ-NR and 8HNQ-NR was reduced by 92% and 55%, respectively, when cells were incubated at 4 ˚C. Similarly, their uptake in the presence of the sodium azide was reduced by 88% and 67%, respectively. The results of the uptake study in the presence of the sodium azide and at 4˚C confirms that the endocytosis of the 6HNQ-NR and 8-HNQ-NR is an active and energy dependent process.

Quantification of the cellular uptake: The percentage cellular uptake of 6HNQ-MF and 8HNQ-NR was studied to obtain information about the amount of molecules entering inside the cells. For this, HeLa cells were seeded in 96 well plates. The cells were treated with 6HNQ-MF and 8HNQ-NR for 6 h, 12 h, and 24 h. The amount of the molecules present outside the cells as well as inside the cells was calculated by making a standard curve for the known amount of the molecules in the growth medium (Figure S16a,b). The percentage of uptake calculated by considering the added amount of the 6HNQ-MF and 8HNQ-NR was found to be 100% (Figure S16c). The results of the study show that in the initial 6 h, uptake of the 6HNQ-MF was 49%, which reached to 67%, and 70% in 12 h and 24h, respectively. Similarly, the 8HNQ-NR showed 79% uptake for 6 h incubation, and following the incubation for 12 h as well as 24 h, no more uptake was noticed beyond 86%.

Long-term cellular imaging: To evaluate the long-term imaging efficiency of **6HNQ-MF** and **8HNQ-NR** inside the cellular environment, HeLa cells were seeded in 6-well plates at a density of 2×10^5 cells/well. Following the attachment, cells were treated with 10 μm of **6HNQ-MF** or **8HNQ-NR** at one time and incubated for 6 h. Cells were washed with PBS and nearly 30% of the cells were further subcultured in the growth medium, whereas the rest of the cells were employed for CLSM imaging. Accordingly, the process was repeated and the CLSM images were recorded. To compare the fluorescence intensity, imaging of the one-time treated cells was carried out at 6 h, 24 h, 48 h, and 72 h. Cells at these time points were washed with PBS, fixed with 4% formaldehyde and images were taken in a confocal microscope using 355 nm laser as an excitation source. The protocol to evaluate the long-term imaging potential of the probes has been schematically presented in Figure S3.

Photostability Study: In this experiment, the photobleaching effect of the long term laser irradiation on **6HNQ-MF** and **8HNQ-NR** was studied. Hela cells at a density of 2 x 10^5

cells/well were treated with 10 μm of **6HNQ-MF** or **8HNQ-NR**. These cells were laser irradiated (405 nm) and images were captured at every 5 min intervals up to 40 min.

Propidium Iodide (PI) Staining for Cell Death Analysis: The population of the dead cells after treatment with IC_{50} concentrations of the **6HNQ-MF** and **8HNQ-NR** separately was studied by PI-based flow cytometric staining. HeLa cells were treated with **6HNQ-MF** or **8HNQ-NR** for 24 h and were collected by trypsinization and centrifugation (700 g, 5 min). After centrifugation, cells were washed with PBS and stained with propidium iodide (2μg/mL) for 20 min. Stained cells were centrifuged to remove residual dye. Following this, cells were suspended in PBS and analyzed in flow cytometer (CytoFLEX, Beckman Coulter) immediately.

DCF-DA Assay for ROS detection: The generation of the ROS was studied by DCF-DA based fluorometric assay. HeLa cells (5 x 10^3/well) were incubated with DCF-DA dye (20 μM) for 1hr. Subsequently, the dye-containing cells were treated with the IC_{50} concentrations of 6HNQ-MF, 8-HNQ-NR, and positive control (H_2O_2). For negative control, a mixture of 6HNQ-MF and N-acetylcysteine (6HNQ-MF+NAC) or 8-HNQ-NR and N-acetylcysteine (8HNQ-NR+NAC) was given to the cells. After 12 h of treatment, cells were gently washed with PBS, and DCF-DA fluorescence intensity (λ_{ex}: 485 nm, λ_{em}: 525 nm) measurements were taken in TECAN multiplate reader. To normalize or remove the fluorescence from the 6HNQ-MF and 8-HNQ-NR molecules, the fluorescence intensities of the 6HNQ-MF and 8-HNQ-NR treated cells were subtracted from DCF-DA stained cells.

JC-1 Staining: The integrity of the mitochondrial membrane was studied by JC-1 dye. The HeLa cells treated with IC_{50} concentrations for 24 h were stained with JC-1 dye (10 μM) for 20 minutes. The measurements of JC-1 monomers (λ_{ex}: 490 nm, λ_{em}: 530 nm) or aggregates (Ex: 525 nm, λ_{em}: 590 nm) were taken in TECAN multiplate reader. The CCCP (Carbonyl cyanide m-chlorophenyl hydrazine) was used as a positive control for depolarization of mitochondrial membrane potential.

Mechanism of Cell Death: Induction of cell death is an important property of the present molecules, which can be further studied for future therapeutic applications. It has been previously reported that the molecules with naphthalimide ring can kill cancer cells and can be used for anticancer therapy.[3,4] Herein, to demonstrate the mechanism of the cell death by NSIs,

DCF-DA assay was performed. As can be seen from Figure S8, the ROS in the 6HNQ-MF and 8HNQ-NR treated cells increased by 2.1 and 1.6 fold, respectively. Along the same line, the treatment of the ROS scavenger (NAC) to the cells with 6HNQ-MF and 8HNQ-NR resulted in decrease in the ROS to the base level. The results show that the NSIs were generating ROS after entering the cells. The generated ROS can damage multiple macro- as well as micro-molecules inside the cells; it also induces mitochondrial membrane damage resulting in the alteration in the mitochondrial membrane potential (MMP). Therefore, we have performed the JC-1 staining to find out the status of MMP after 6HNQ-MF and 8HNQ-NR treatment (Figure S9). The JC-1 dye forms aggregates in the polarized mitochondria giving orange/red fluorescence while remains in the non-aggregated or monomeric form in depolarized mitochondria. The ratio of the JC-1 aggregates to monomer fluorescence (JC-1 A/M) was used as an indicator of mitochondria's health. The results in the Figure S9 shows that JC-1 A/M ratios for the untreated HeLa cells were 1.23 to 1.69, which were further reduced to 0.87 and 1.03 after treatment with the IC50 concentrations of the 6HNQ-MF and 8HNQ-NR, respectively. In summary, the generation of the ROS must have induced damaging-effects on biological macromolecules, including mitochondrial membrane, which ultimately results into the depolarization of MMP. The depolarized mitochondria activates the proteins involved in the apoptosis, and cells undergo death by apoptosis process. It is well documented that the most common features of apoptotic cell death are the DNA damage, cell shrinkage, and membrane blebbing. In our study, the apoptotic cell death was established from the membrane blebbing in FESEM images of HeLa cells treated at IC50 concentration (Figure S10-S12). The FESEM image of the treated cells along with the generation of ROS and depolarization of the MMP confirmed cell death induction or the anti-cancerous properties of the NSIs.

Synthetic route

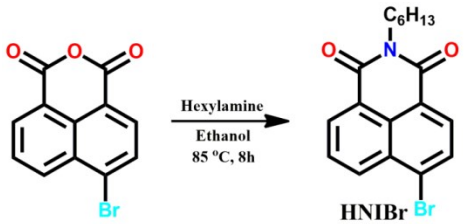

Scheme S1. The synthetic procedure used to prepare probe HNIBr.

Synthetic Procedure for Alkylation: To a suspension of 4-bromonaphthalene anhydride (554.2 mg, 2 mmol) in ethanol, hexylamine (146.28 mg, 2 mmol) was added dropwise at room temperature. The temperature was increased and stirred for 8 hours at 85 °C. The mixture was cooled and the solvent was evaporated under reduced pressure. The solid residue was dissolved in chloroform and washed with water two times. The organic layer was concentrated after drying over anhydrous Na_2SO_4. Finally, column chromatography was performed to obtain the pure product (**HNIBr**).

Characterization data of HNIBr: Light green solid (615 mg, 85% yield); HRMS (*m/z*): calcd for $C_{18}H_{18}BrNO_2$ 359.0521; found 360.0600 $[M+H]^+$; ^1H NMR (600 MHz, $CDCl_3$, δ ppm) 8.57 (d, 1H), 8.46 (d, 1H), 8.32 (d, 1H), 7.94 (d, 1H), 7.77 (t, 1H), 4.12 (t, 2H) 1.70 (m, 2H), 1.31 (m, 6H), 0.87 (t, 3H); ^{13}C NMR (150.00 MHz, $CDCl_3$, δ ppm) 163.63, 163.60, 133.22, 132.06, 131.25, 131.16, 130.61, 130.24, 128.98, 128.15, 123.21, 122.34, 40.78, 31.71, 28.18, 26.96, 22.74, 14.25.

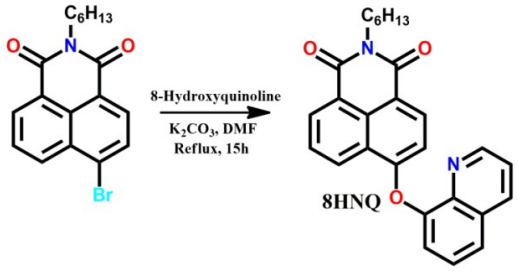

Scheme S2. The synthetic scheme for 8HNQ.

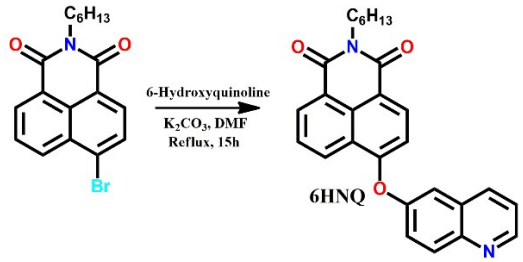

Scheme S3. The synthetic scheme for 6HNQ.

Synthetic Procedure for 8HNQ and 6HNQ: To different round bottom flasks, each containing the solution of **HNIBr** (0.5 mmol) in DMF (5 mL), 1 mmol of the respective hydroxyquinoline (8-hydroxyquinoline for **8HNQ** and 6-hydroxyquinoline for **6HNQ**) and 200 mg of K_2CO_3 were added to them separately and were refluxed for 15 hours. The solvents were vaporized under vacuum and the residues were extracted with chloroform (30×3 mL). The organic layers were washed with H_2O several times followed by washing with brine and dried over anhydrous Na_2SO_4. The crude products were concentrated and purified through column chromatography over silica gel to get the final products (**8HNQ** and **6HNQ**) respectively.

Characterization data for 8HNQ: Yellow solid (155 mg, 73% yield); M.p. 168-170 ^oC; HRMS (*m/z*): calcd for $C_{27}H_{24}N_2O_3$ 424.1787; found 425.1894 $[M+H]^+$; ^1H NMR (600 MHz, $CDCl_3$, δ ppm) 8.85 (d, 2H), 8.64 (d, 1H), 8.37 (d, 1H), 8.24 (d, 1H), 7.76-7.79 (m, 2H), 07.57 (t, 1H), 7.46 (d, 2H), 6.72(d, 1H), 4.14 (t, 2H), 1.70 (m, 2H), 1.32 (m, 6H), 0.86 (t, 3H), ^{13}C NMR (150.00 MHz, $CDCl_3$, δ ppm) 164.58, 163.93, 160.51, 151.11, 150.91, 141.31, 136.42, 132.84, 131.95, 130.24, 129.81, 129.16, 126.89, 126.62, 125.63, 123.91, 122.72, 122.29, 120.32, 116.84, 111.39, 40.53, 31.72, 28.25, 26.97, 22.73, 14.25.

Characterization data for 6HNQ: Yellow solid (140 mg, 66% yield); HRMS (*m/z*): calcd for $C_{27}H_{24}N_2O_3$ 424.1787; found 425.1861 $[M+H]^+$; ^1H NMR (600 MHz, $CDCl_3$, δ ppm) 8.94 (s, 1H), 8.69 (dd, 2H), 8.49 (d, 1H), 8.24 (d, 1H), 8.11 (d, 1H), 7.81 (t, 1H), 7.59 (dd, 1H), 7.53 (d, 1H), 7.46 (dd, 1H), 7.02 (d, 1H), 4.18 (t, 2H), 1.73 (m, 2H), 1.34 (m, 6H), 0.89 (t, 3H), ^{13}C NMR (150.00 MHz, $CDCl_3$, δ ppm) 164.48, 163.85, 162.78, 159.31, 153.33, 150.37, 135.77, 132.80, 132.42, 132.19, 129.96, 128.57, 126.98, 124.32, 123.99, 123.02, 122.17, 122.13, 117.65, 116.61, 111.94, 40.67, 31.75, 28.29, 26.99, 22.76, 14.24.

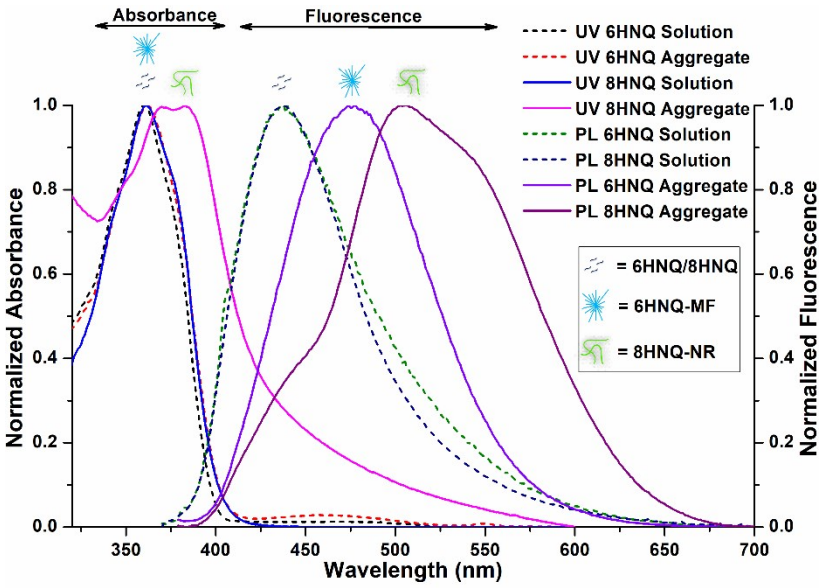

Figure S1. Normalized UV-Visible and fluorescence spectra of 6HNQ and 8HNQ in solution (in DMF) as well as aggregated state (at 99.8% water in DMF).

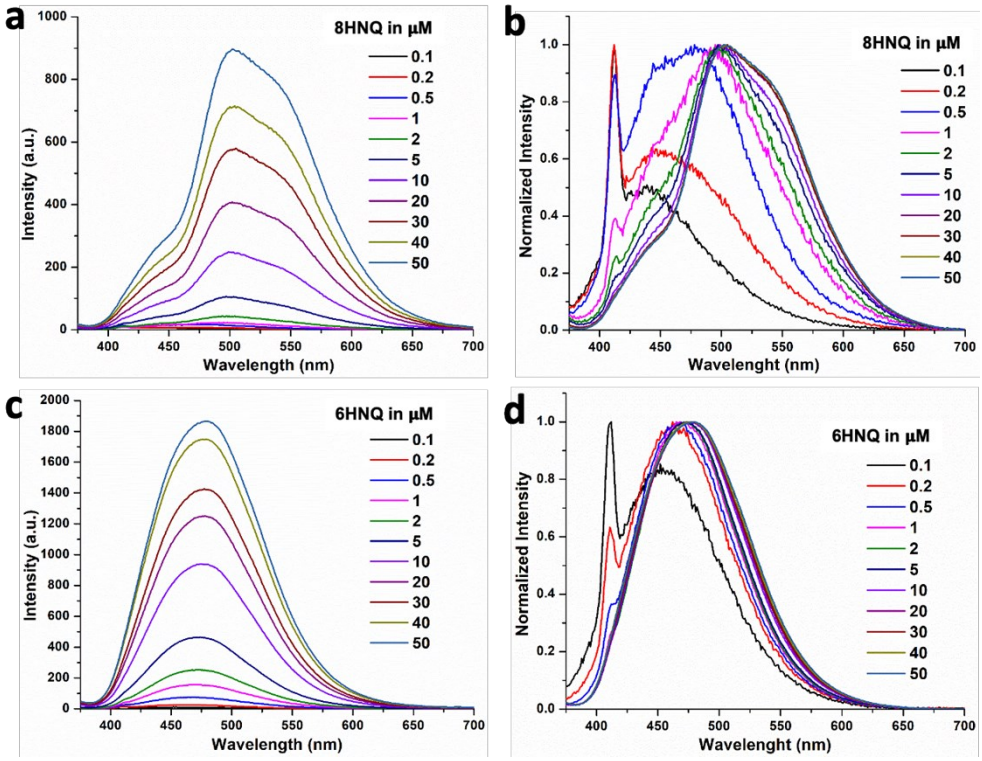

Figure S2. Concentration dependent fluorescence spectra of (a) 8HNQ and (c) 6HNQ in 99.5-99.9% f_w in DMF and their respective (b,d) normalized fluorescence spectra (λ_{ex} = 360 nm).

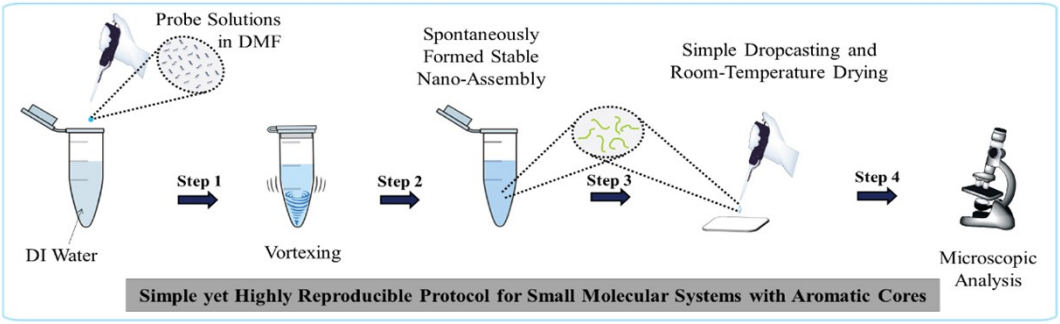

Figure S3. Schematic representation of the highly reproducible, cost-effective, and practically simple drop-casting technique to generate the supramolecular self-assemblies from the NSIs.

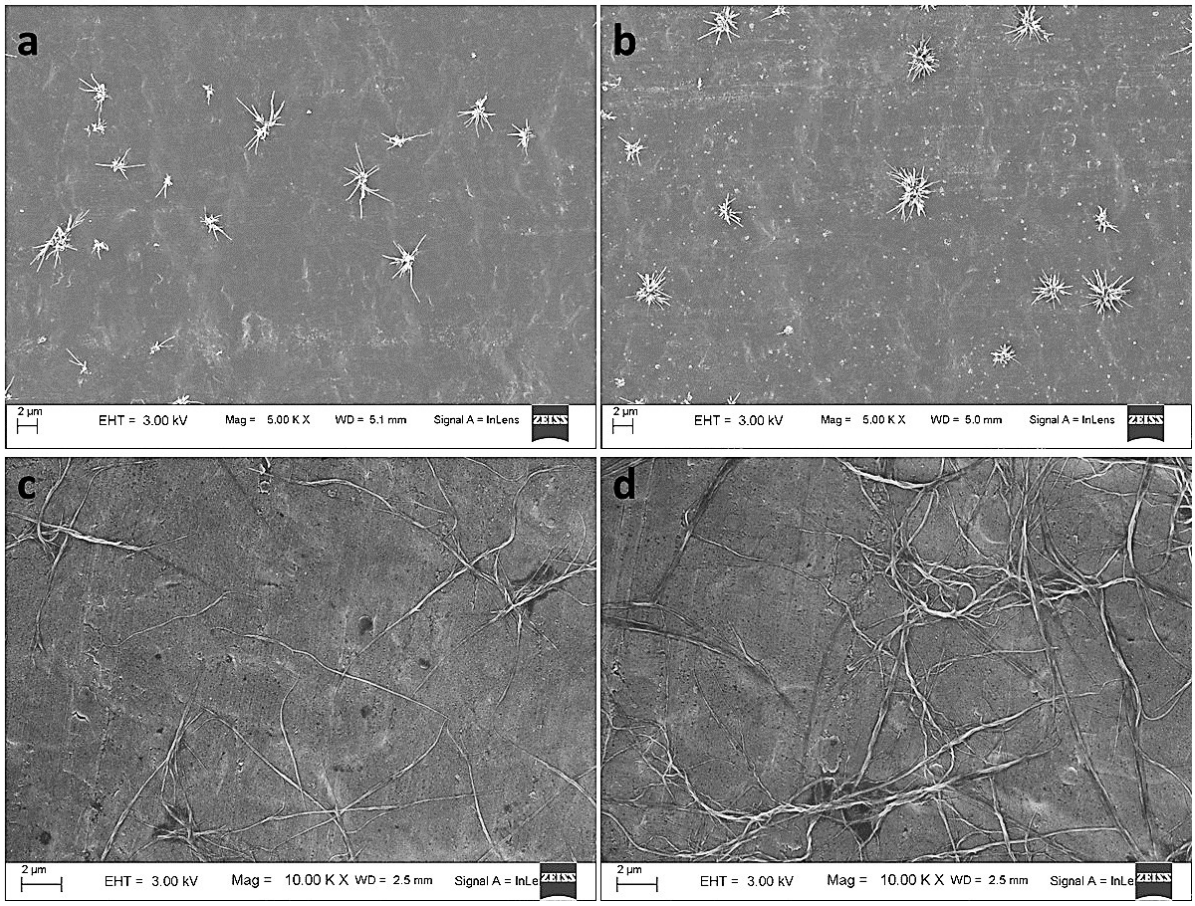

Figure S4. FESEM images of the 6HNQ at 10 µM (a) and 20 µM (b) concentration. Similarly FESEM images of the 8HNQ at 10 µM (c) and 20 µM (d) concentration.

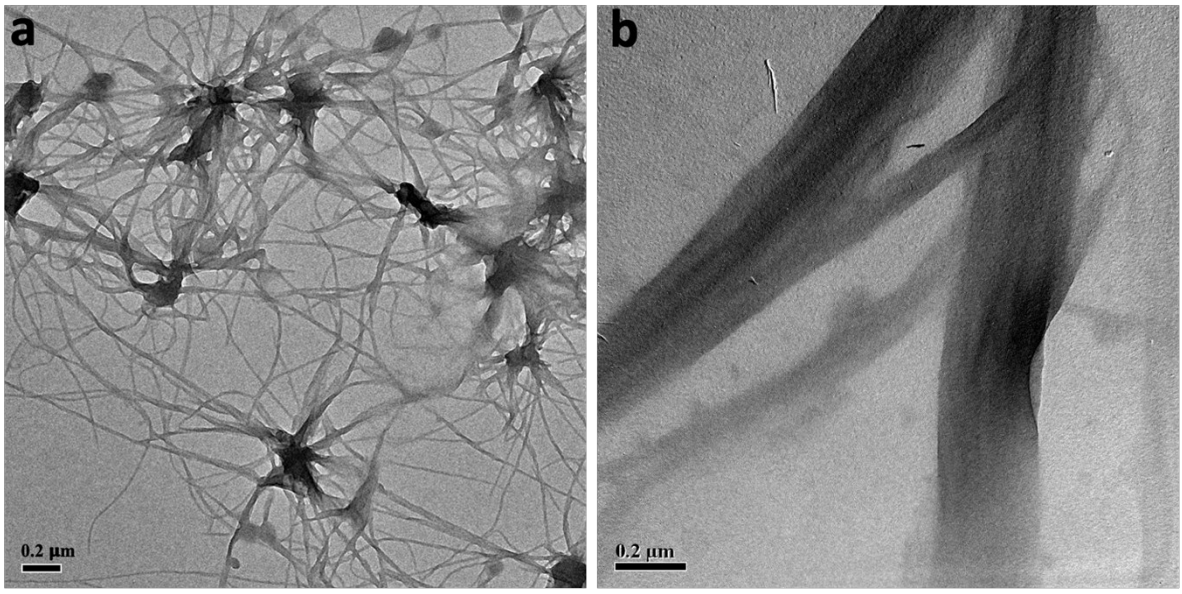

Figure S5. TEM images of spontaneously self-assembled (left) 6HNQ-MF and (right) 8HNQ-NR at 99.8% f_w in DMF (20 μM).

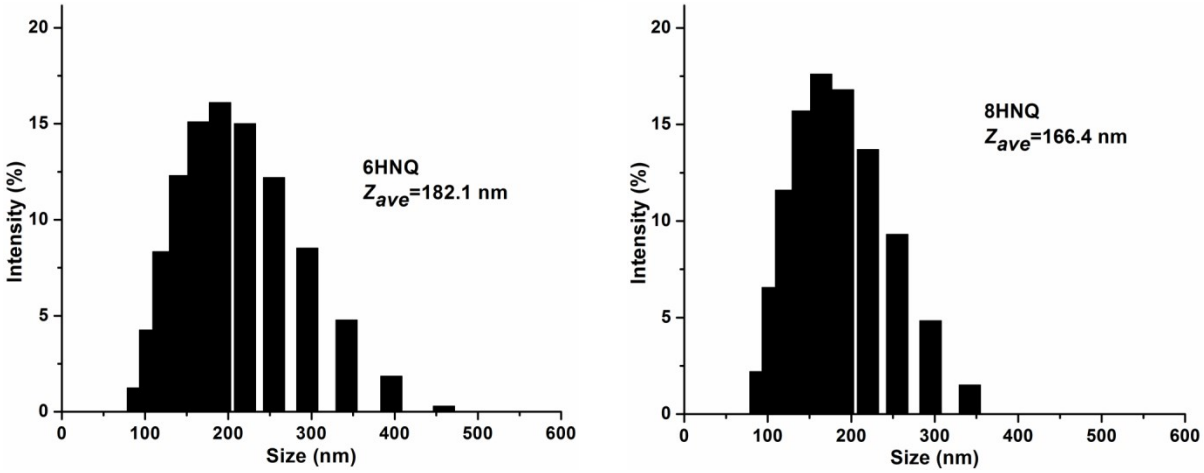

Figure S6. Size distribution of 6HNQ and 8HNQ nanoaggregates (10 μM) by DLS measurements in water at 25 °C.

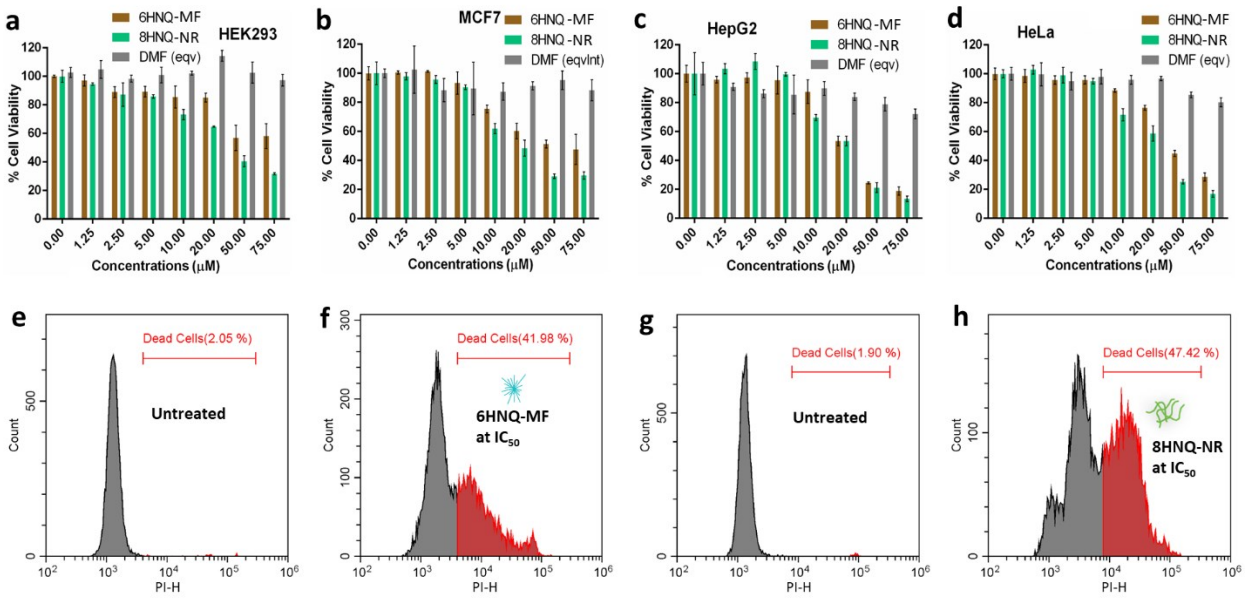

Figure S7. Cell viability and quantitative apoptosis of the conformational isomers with distinct supramolecular self-assembly. (a-d) Cell viability of 6HNQ-MF, 8HNQ-NR, and DMF (volume eqv.) against HEK293, MCF7, HepG2, and HeLa cells (24 h of incubation). (e-h) Quantitative cell death analysis of HeLa cells with the treatment of IC50 concentrations of 6HNQ-MF and 8HNQ-NR separately by propidium iodide-based flow cytometric assay. See also Table S1, Figure S5-S7.

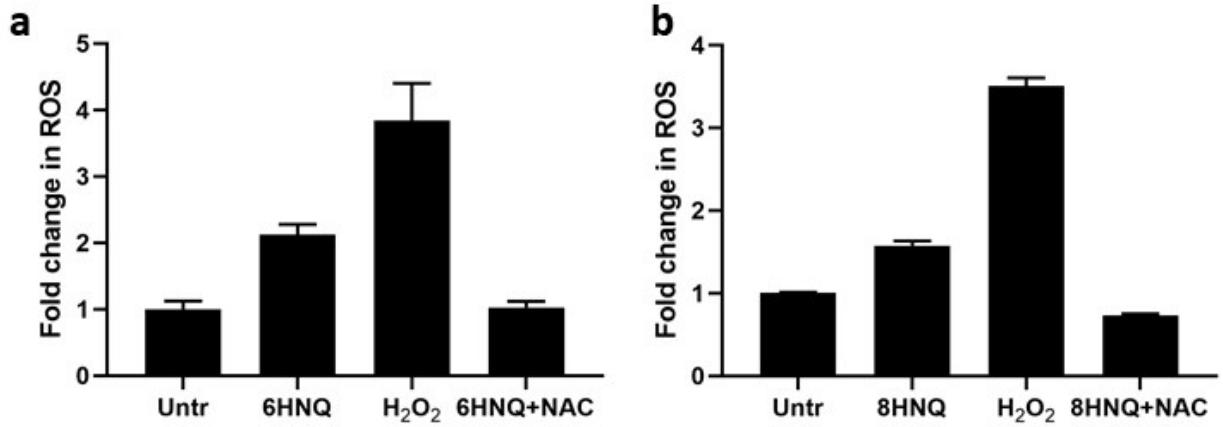

Figure S8. DCF-DA assay results for (a) 6HNQ-MF and (b) 8NHQ-NR treatment on HeLa cells. H_2O_2 was used as a positive control, while N-acetylcysteine (NAC) was used a negative control for ROS generation.

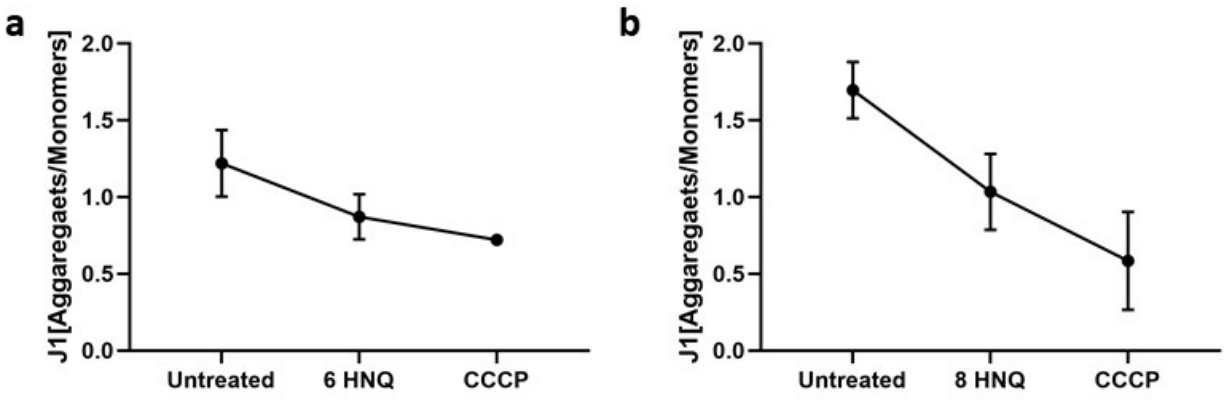

Figure S9. The JC-1 staining results for (a) 6HNQ-MF and (b) 8HNQ-NR treatment on HeLa cells for 24 h.

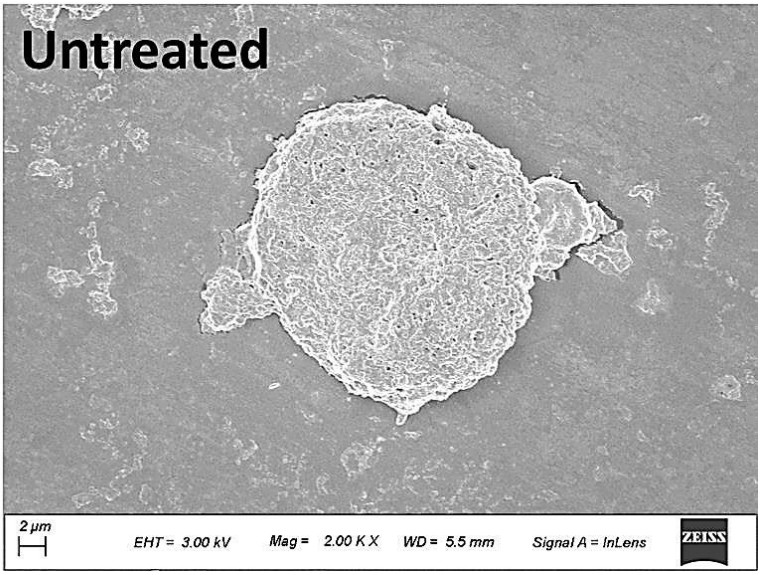

Figure S10. FESEM images of untreated HeLa cells.

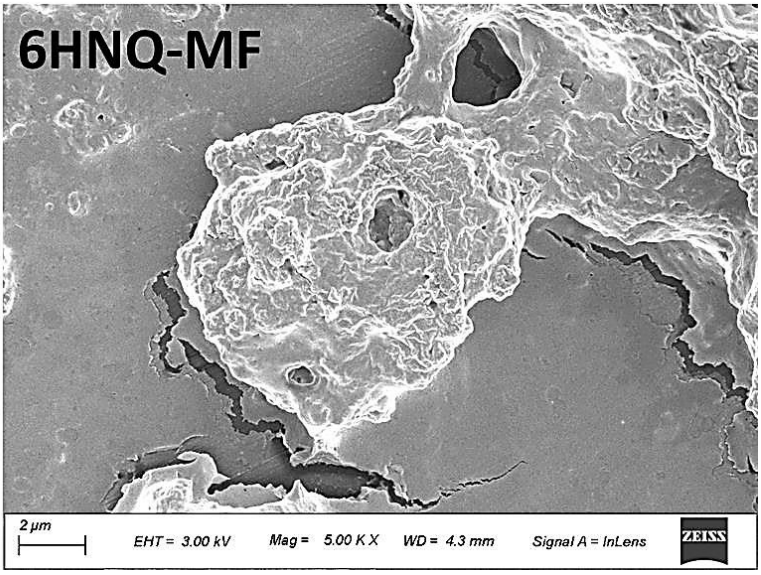

Figure S11. FESEM images of HeLa cells treated with 6HNQ-MF at IC_{50} concentration.

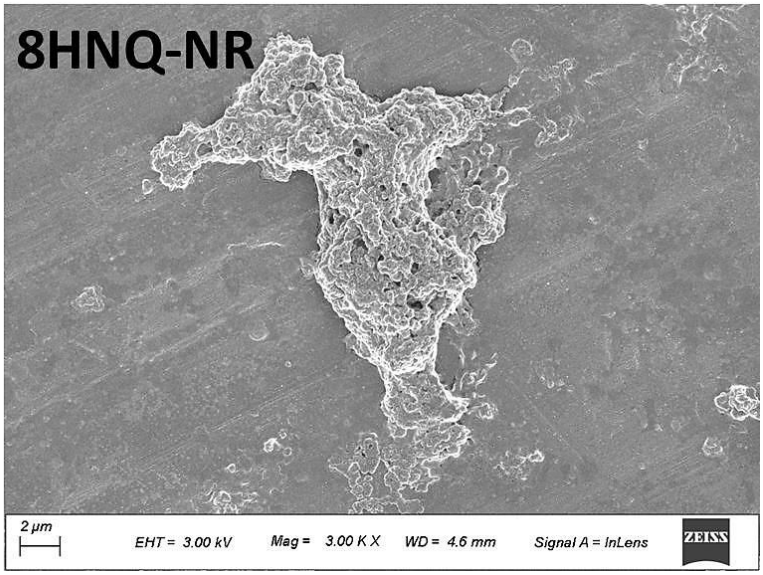

Figure S12. FESEM images of HeLa cells treated with 8HNQ-NR at IC_{50} concentration.

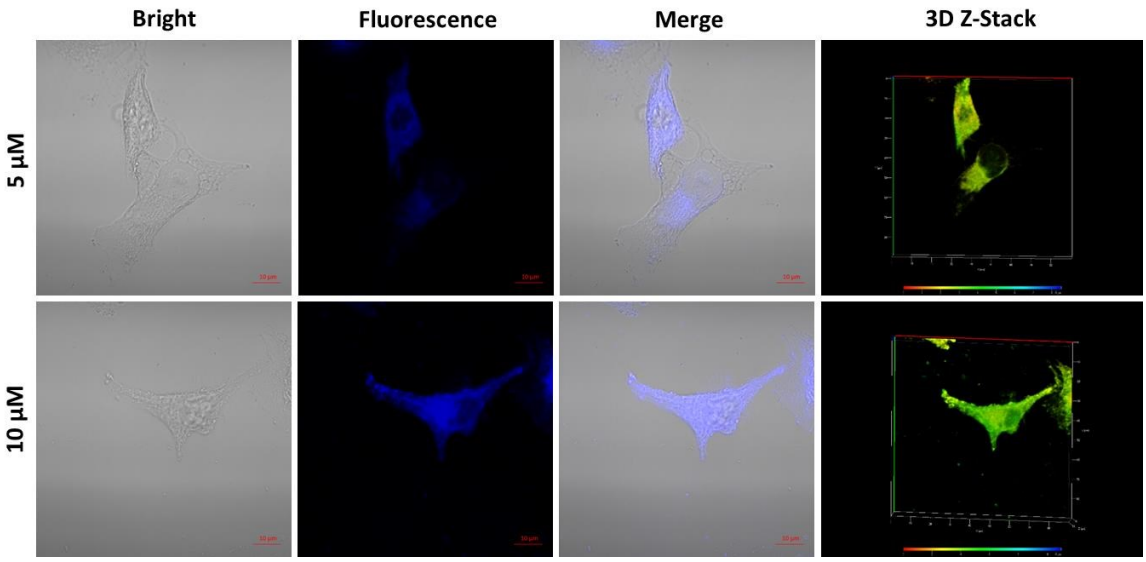

Figure S13. CLSM images of HeLa cells incubated with 6HNQ-MF for 5 h at different concentrations. 3D Z-stack images showing complete accumulation of the probe into the cells.

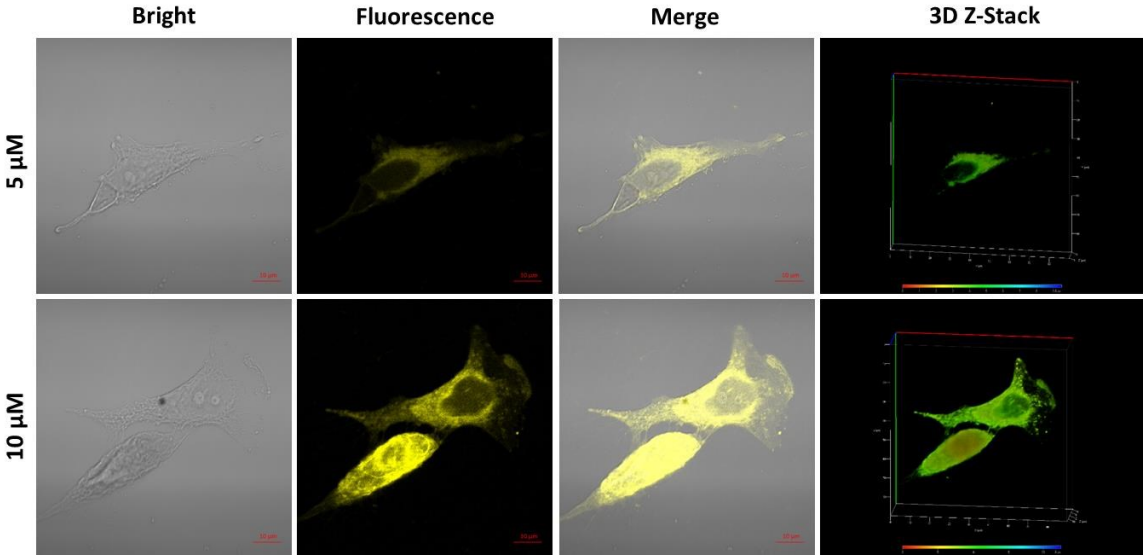

Figure S14. CLSM images of HeLa cells incubated with 8HNQ-NR for 5 h at different concentrations. 3D Z-stack images showing complete accumulation of the probe into the cells.

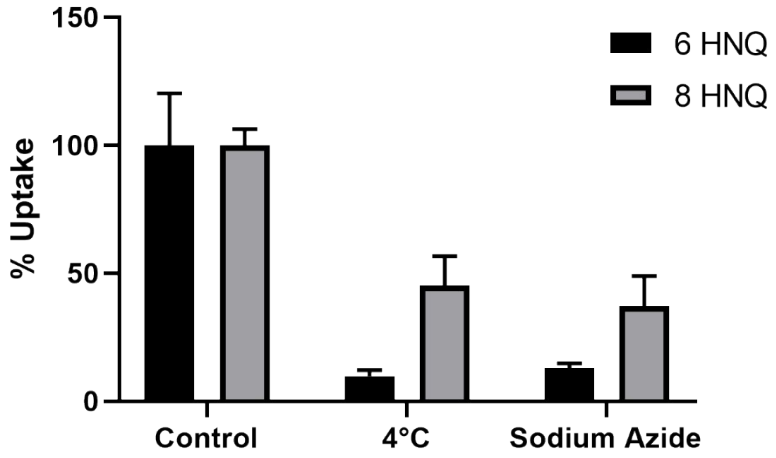

Figure S15. Comparison of the uptake of the 6HNQ-MF and 8HNQ-NR with or without 4˚C and sodium azide treatment.

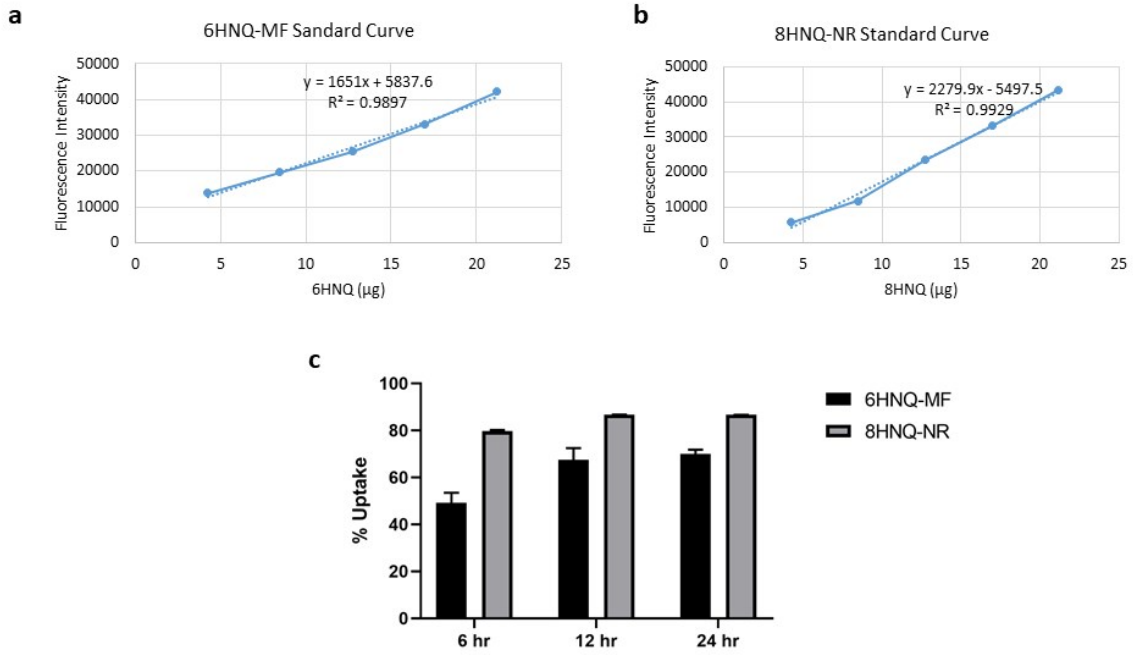

Figure S16. (a,b) Standard curve for the known amount 8HNQ-NR and 6HNQ-MF in the growth medium. (c) Uptake % of 8HNQ-NR and 6HNQ-MF at different time point.

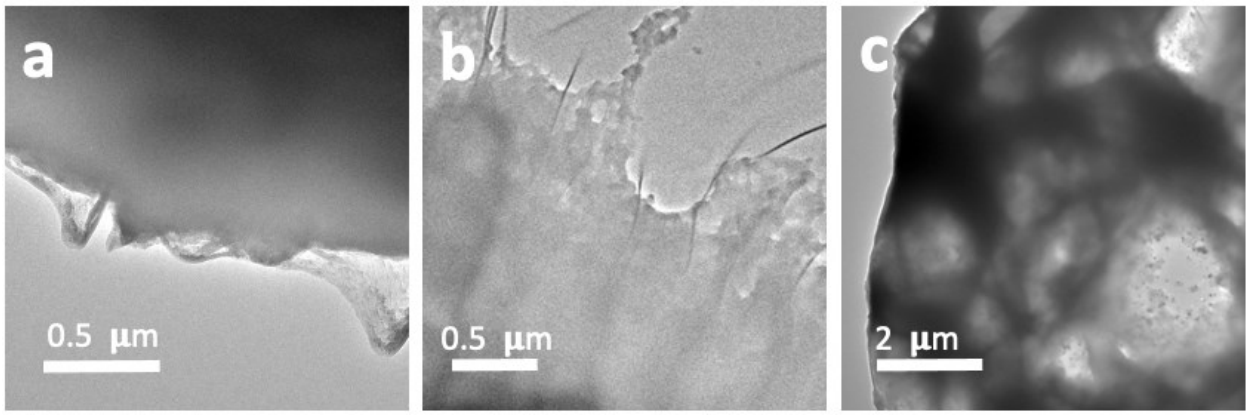

Figure S17. TEM images of cell (a) without probe treatment, and with the treatment of (b) 6HNQ-MF and (c) 8HNQ-NR for 8 h.

Characterization Spectra for synthesized molecules

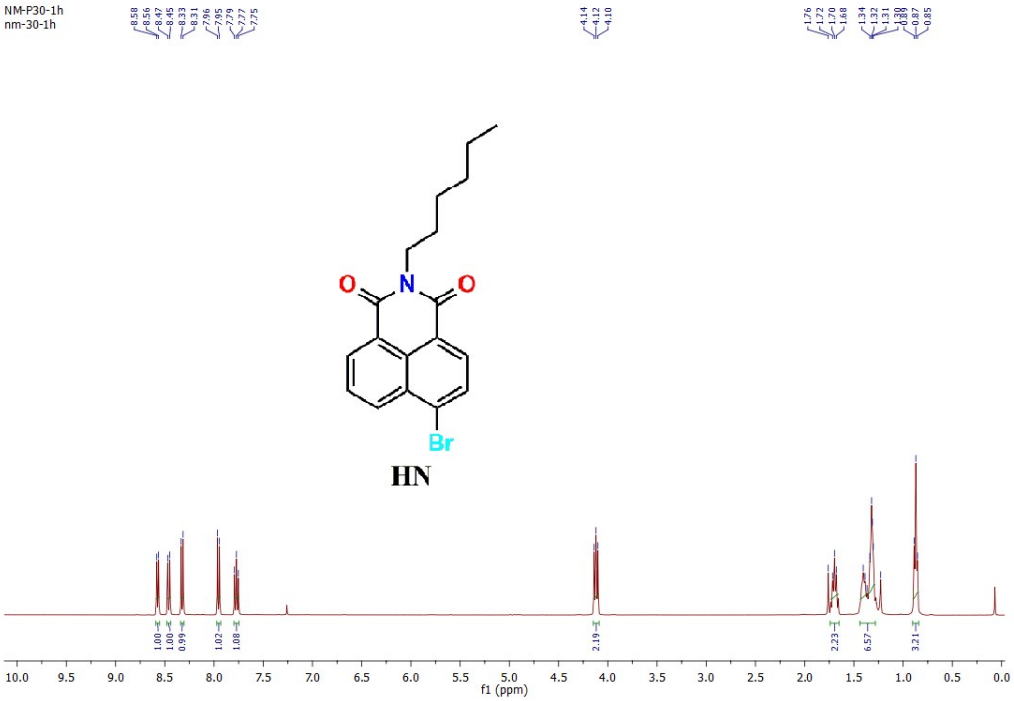

^{1}H NMR Spectra of HN

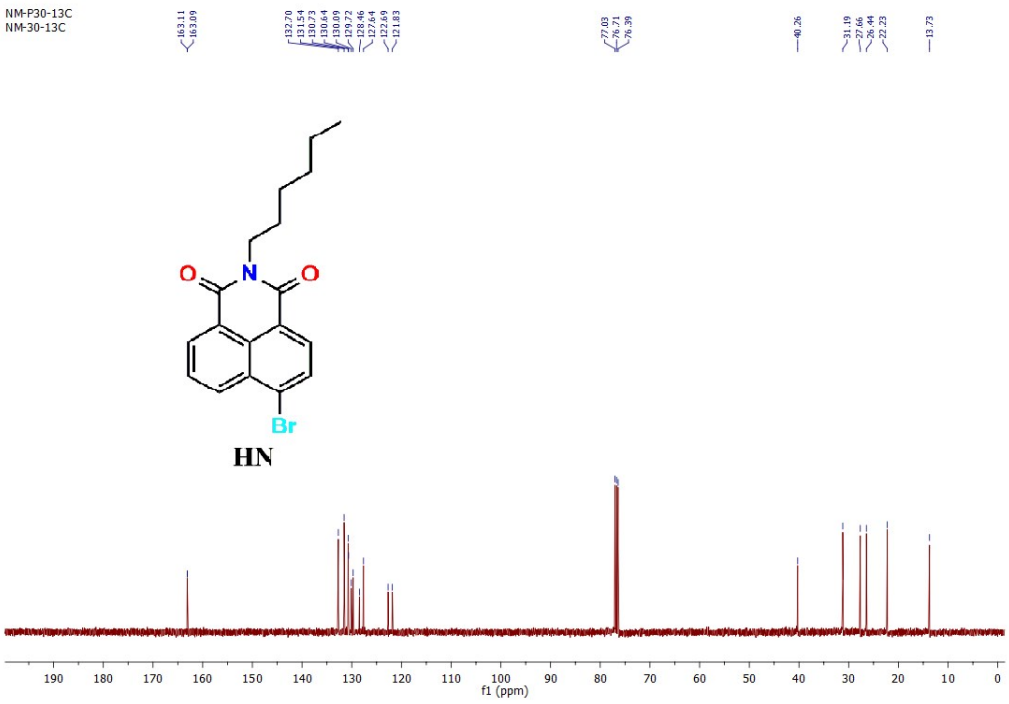

^{13}C NMR Spectra of HN

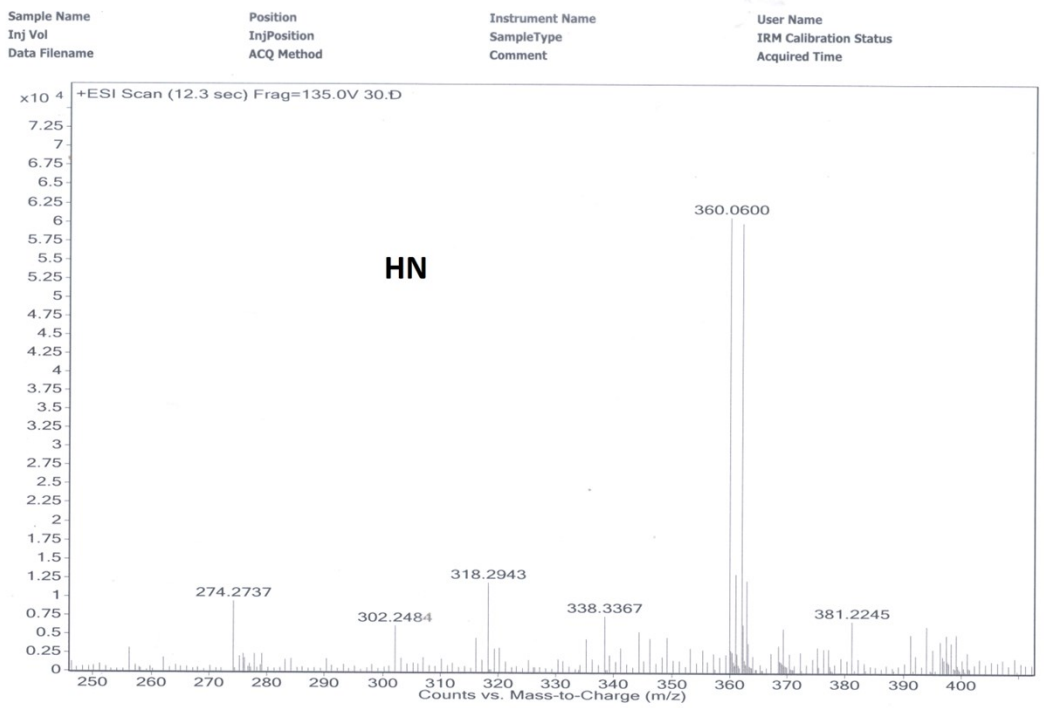

HRMS of HN

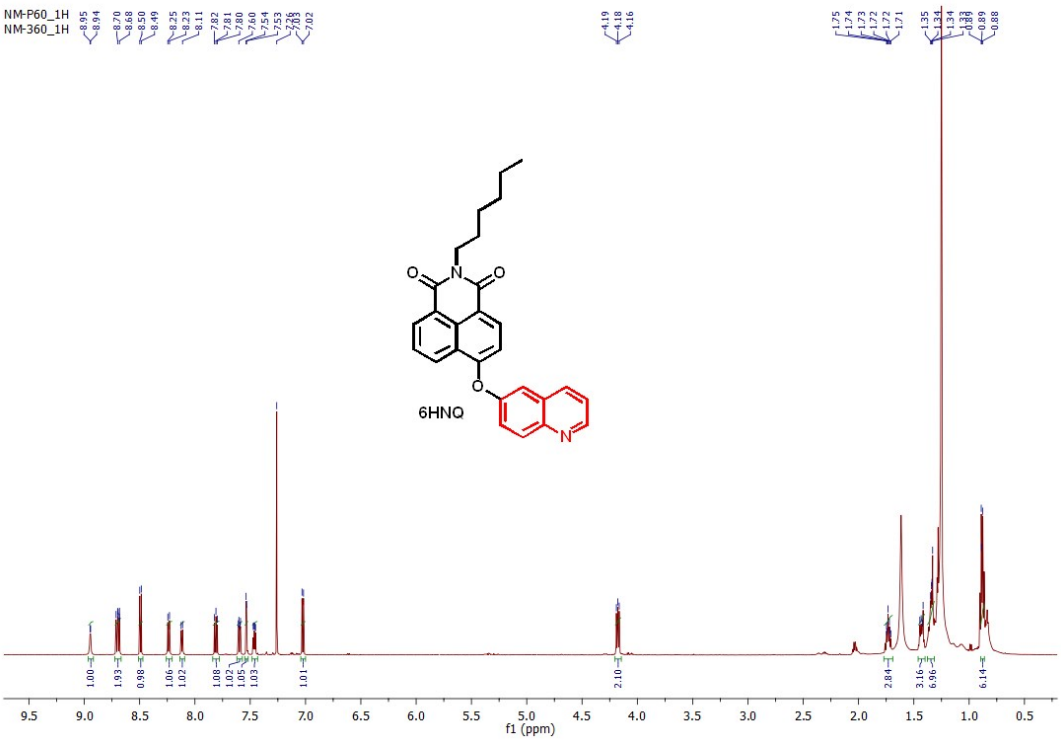

^{1}H NMR Spectra of 6HNQ

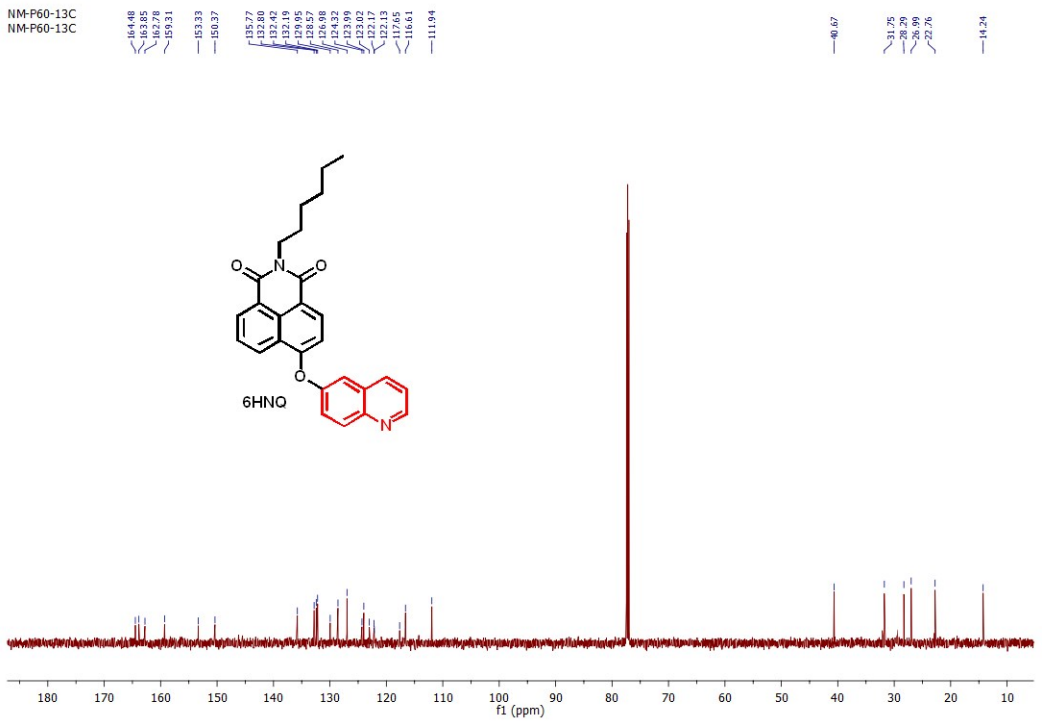

^{13}C NMR Spectra of 6HNQ

Sample Name	NM-P-60	**Position**	Vial 1	**Instrument Name**	QTOF	**User Name**	
Inj Vol	-1	**InjPosition**		**SampleType**	Sample	**IRM Calibration Status**	Success
Data Filename	NM-P-60.d	**ACQ Method**		**Comment**		**Acquired Time**	8/31/2018 5:03:55 PM

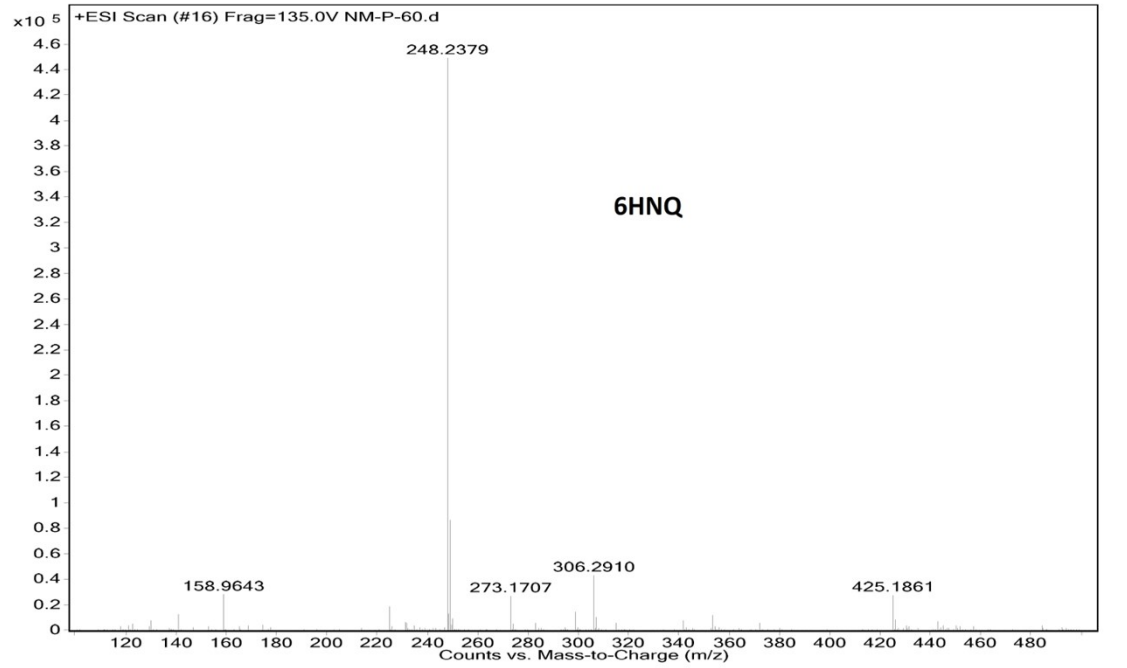

HRMS of 6HNQ

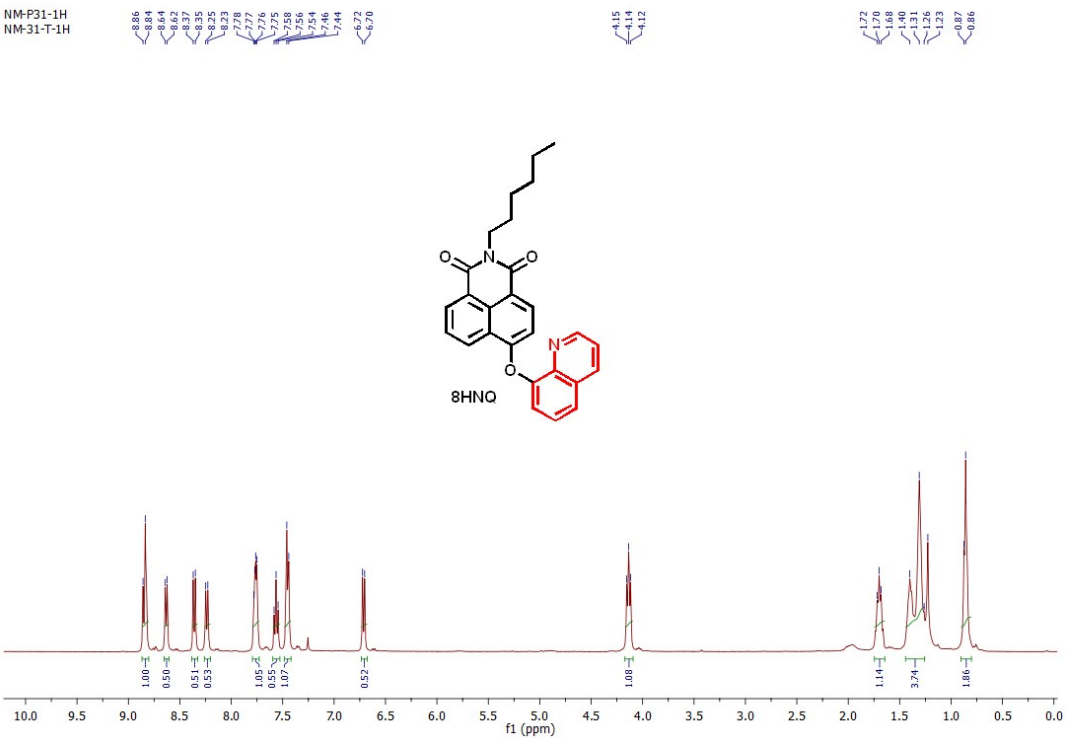

^{1}H NMR Spectra of 8HNQ

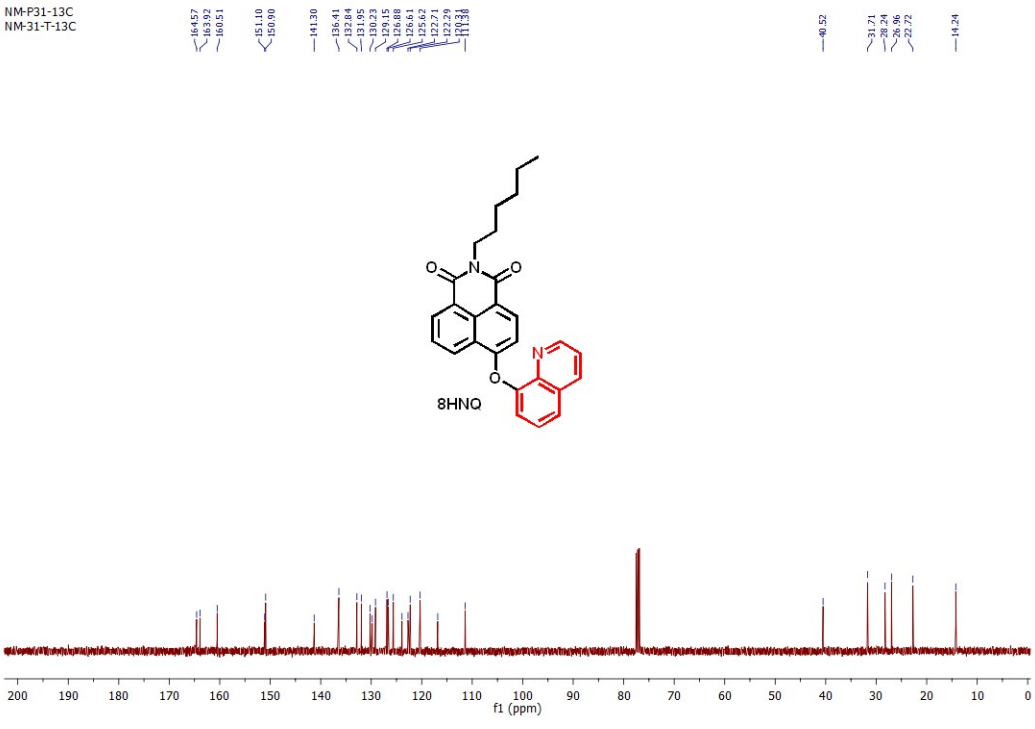

^{13}C NMR Spectra of 8HNQ

Sample Name	NM-31-T	**Position**	Vial 1	**Instrument Name**	Instrument 1	**User Name**	
Inj Vol	-10	**InjPosition**		**SampleType**	Sample	**IRM Calibration Status**	Success
Data Filename	NM-31-T.d	**ACQ Method**		**Comment**		**Acquired Time**	10/13/2015 2:44:09 PM

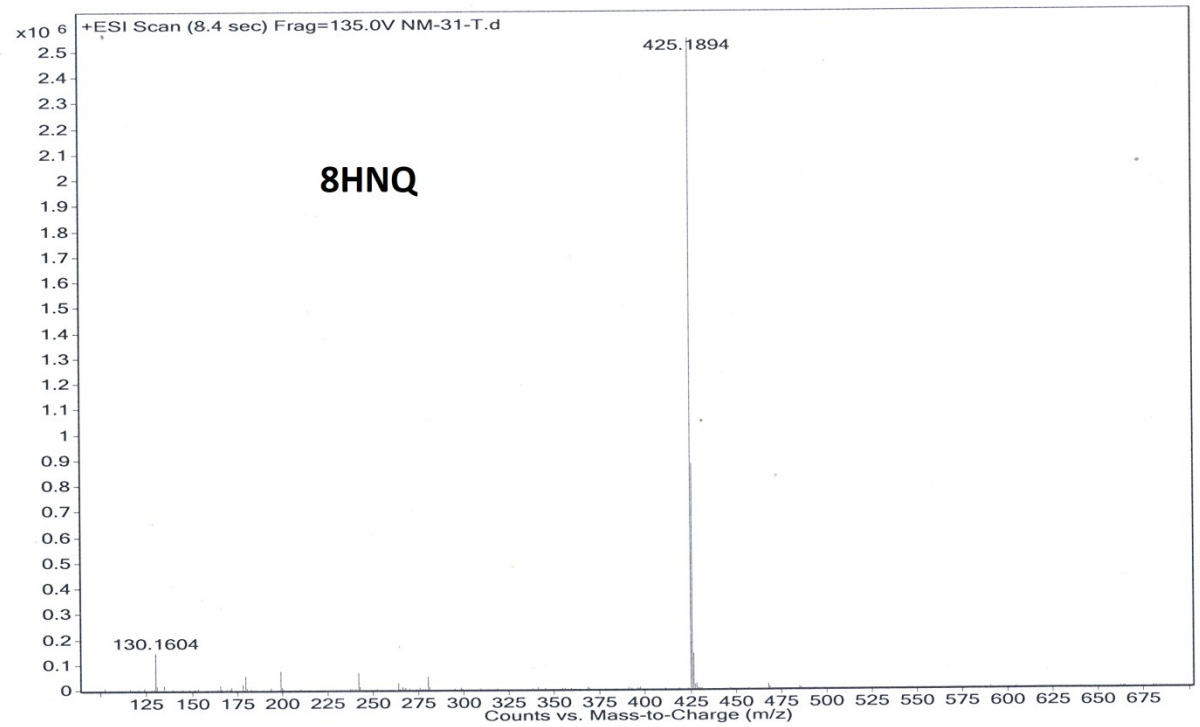

HRMS of 8HNQ

References

(1) Becke, A. D. *J. Chem. Phys.* **1993**, *98*, 5648.

(2) Frisch, M. J.; Trucks, G. W.; Schlegel, H. B.; Scuseria, G. E.; Robb, M. A.; Cheeseman, J. R.; Scalmani, G.; Barone, V.; Mennucci, B.; Petersson, G. A.; Nakatsuji, H.; Caricato, M.; Li, X.; Hratchian, H. P.; Izmaylov, A. F.; Bloino, J.; Zheng, G.; Sonnenberg, J. L.; Hada, M.; Ehara, M.; Toyota, K.; Fukuda, R.; Hasegawa, J.; Ishida, M.; Nakajima, T.; Honda, Y.; Kitao, O.; Nakai, H.; Vreven, T.; Montgomery, J. A.; Jr., Peralta, J. E.; Ogliaro, F.; Bearpark, M.; Heyd, J. J.; Brothers, E.; Kudin, K. N.; Staroverov, V. N.; Kobayashi, R.; Normand, J.; Raghavachari, K.; Rendell, A.; Burant, J. C.; Iyengar, S. S.; Tomasi, J.; Cossi, M.; Rega, N.; Millam, J. M.; Klene, M.; Knox, J. E.; Cross, J. B.; Bakken, V.; Adamo, C.; Jaramillo, J.; Gomperts, R.; Stratmann, R. E.; Yazyev, O.; Austin, A. J.; Cammi, R.; Pomelli, C.; Ochterski, J. W.; Martin, R. L.; Morokuma, K.; Zakrzewski, V. G.; Voth, G. A.; Salvador, P.; Dannenberg, J. J.; Dapprich, S.; Daniels, A. D.; Farkas, O.; Foresman, J. B.; Ortiz, J. V.; Cioslowski, J.; Fox, D. J. *Gaussian 09, Revision A.02, Gaussian, Inc., Wallingford CT*, **2009**.

3. Banerjee, S.; Veale, E. B.; Phelan, C. M.; Murphy, S. A.; Tocci, G. M.; Gillespie, L. J.; Frimannsson, D. O.; Kelly, J. M.; Gunnlaugsson, T. *Chem. Soc. Rev*., **2013**, *42*, 1601-1618.

4. Duke, R. M.; Veale, E. B.; Pfeffer, F. M.; Kruger, P. E.; Gunnlaugsson, T. *Chem. Soc. Rev.,* **2010**, *39*, 3936–3953.